Molecular dynamics simulations of shock-induced deformation twinning of a body-centered-cubic metal

A. Higginbotham,[1] M. J. Suggit,[1,*] E. M. Bringa,[2] P. Erhart,[3] J. A. Hawreliak,[3] G. Mogni,[1] N. Park,[4] B. A. Remington,[3] and J. S. Wark[1]

[1]*Department of Physics, Clarendon Laboratory, University of Oxford, Parks Road, Oxford OX1 3PU, United Kingdom*
[2]*CONICET & Instituto de Ciencias Básicas, Universidad Nacional de Cuyo, Mendoza 5500, Argentina*
[3]*Lawrence Livermore National Laboratory, Livermore, California 94550, USA*
[4]*Atomic Weapons Establishment, Aldermaston, Reading RG7 4PR, United Kingdom*

(Received 17 April 2013; published 17 September 2013)

Despite a number of previous nonequilibrium molecular dynamics (MD) studies into plasticity in face-centered-cubic metals, and phase transitions in body-centered-cubic (bcc) metals, the plastic response to rapid compression of bcc metals remains largely unexplored. Key questions remain as to the relative importance of dislocation motion and twinning in shear stress release and consequent strength. We present here large scale MD simulations of shock compressed bcc metal, using an extended Finnis-Sinclair potential for tantalum, and demonstrate the presence of significant deformation twinning for pressures above the Hugoniot elastic limit for shock waves propagating along the [001] direction. The twinned variants are separately identified by a per atom order parameter, allowing the strain and stress states of the rotated material to be studied. The atomic motion during twinning, and thus its mechanism, for this potential, is identified by use of a three-dimensional pair-correlation function.

DOI: 10.1103/PhysRevB.88.104105 PACS number(s): 62.50.Ef, 61.72.Mm

I. INTRODUCTION

The plastic response of materials undergoing shock compression has been the subject of extensive computational and experimental study.[1–8] To date, much of the progress has been in our understanding of face-centered-cubic (fcc) materials where dislocation generation and flow is the dominant mechanism governing plasticity. In these materials (copper often being considered an archetypal fcc metal) the homogenous nucleation of dislocations,[1,4] their motion, and ultimate pinning,[3] leading to strength, have been reported in molecular dynamics (MD) simulations for a over decade. In addition to computational efforts, experiments have recorded *in situ* x-ray diffraction from Cu shocked to pressures of 100 GPa.[5] The remarkable degree of qualitative and, in many cases, quantitative agreement between MD and experiment (especially laser driven shock compression where both length and time scales are close to commensurate with MD) has given increased confidence in the use of such simulations as both predictive and interpretative tools.

Despite the wealth of information available for fcc metals, the response of body-centered-cubic (bcc) materials to shock compression has received less attention. This is due in large part to the relative paucity of potentials which are able to faithfully describe non-close-packed metallic bonding. Remarkable success has been achieved in the modeling of Fe, where large scale molecular dynamics simulations predicted the α-ε phase transition under shock compression of single crystal samples,[9] in agreement with experiments for the response for shock compression along the (001) axis.[10,11] However, even here, simulations of shocks along other crystallographic directions,[9] and in polycrystals,[12] have produced highly unexpected results (that is to say, the prediction of a shock-induced fcc, as well as hcp, phase) which have not been verified by experiment.[13] Although the veracity of these results are still a matter of ongoing study, it is clear that one must be careful to verify the often complex behavior of these potentials. A recent study compared four different potentials for Fe, finding a different resulting microstructure under pressure.[14] That said, the relatively sparse experimental data set for *in situ* microstructural measurements during shock compression make this a challenging prospect.

In this paper we chose tantalum as the bcc metal of study. Tantalum is a particularly complex material due to its multitude of plasticity mechanisms (a combination of dislocation and deformation twinning mediated responses) as well as the α-ω phase transition. The majority of published work outlining microstructural response focuses on polycrystals. Early work showed that impact and low strain rate compressive testing at cryogenic temperatures led to work hardening due to twinning.[15] However, equivalent room temperature studies saw comparatively little evidence that twinning occurred upon deformation.[16] Early recovery work on explosively driven shocks with peak pressures of 45 GPa showed profuse twinning about the {112} planes.[17] In other work, shock pressures of 15 GPa showed a combination of dislocation activity and twinning in recovered polycrystalline samples, with 45 GPa shocks also producing residual regions of the metastable ω phase.[18] The same work failed to find evidence of twinning or ω phase material in single crystals oriented along [011] for either pressure. Subsequent work found evidence of dislocation activity and twinning in single crystal samples shock compressed along several different orientations, although twin fractions varied considerably between orientations with relative abundances showing a strong pressure dependence.[19]

In this paper we use large scale MD simulations to investigate the response of bcc material to rapid, uniaxial loading along [001] with the aim of initiating deformation twinning. We find that the material responds plastically above a piston velocity of 0.8 km s^{-1} via massive deformation twinning in the $\{112\}\langle 111\rangle$ system. A per atom parameter is developed which allows atoms in each twin orientation to be isolated,

allowing the strain and stress within the twins to be determined. We find that although the bulk of the initial one-dimensional (1D) strain is relieved, the twins still support a significant shear stress. However, this shear stress is considerably smaller than the global shear stress as would be measured experimentally. Finally we determine the mechanism for twinning in these simulations. Given the relatively simple nature of the potential used, we do not claim to exactly model what will occur in shocked Ta, however, the observed mechanism provides an idea for how twinning of bcc materials may occur under shock compression.

II. SIMULATIONS

In order to investigate deformation twinning under shock compression we employ large scale molecular dynamics simulations using the LAMMPS code.[20] Samples of size up to $140 \times 140 \times 2000$ cells ($462 \times 462 \times 6605$ Å^3) were initially thermalized to 5 K before being dynamically compressed by driving a piston along the z direction at a fixed velocity U_p into the material. This low starting temperature was chosen both to allow easier visualization of the twins, and to encourage twinning as the dominant mechanism. Simulations were also performed after thermalizing to 300 K, with qualitatively similar results. Periodic boundary conditions were used for the transverse directions.

For shock simulation a key consideration is always the choice of potential. Very few potentials are designed specifically to be well matched to high pressure data pertinent to shock compression, and fewer still are able to capture the partial filling of the d orbitals which stabilizes Ta in its bcc phase. Ravelo *et al.* have recently presented a new embedded atom method (EAM) Ta potential for high pressure studies,[21] however, in this paper we made use of the extended Finnis-Sinclair (EFS) potential.[22] More complex potentials exist, for example, model generalized pseudopotential theory (MGPT),[23] but their relative computational expense makes them undesirable for many large scale studies, and this may be worthy of future investigation. The EFS potential produces a good match to both the zero pressure phonon dispersion curves and to the high pressure elastic constants. Figure 1 compares the shock Hugoniot derived from our simulations for shocks along [001] using the EFS potential with experimental data,[24,25] showing excellent agreement.

For particle velocities below $U_p = 0.8$ km s^{-1} the predicted response of the material is elastic (as evinced by the lack of shear stress relief in the uniaxially compressed bcc structure). However, at $U_p \geqslant 0.8$ km s^{-1}, shear stress [defined as a simplified von Mises stress, $\sigma_s = \sigma_{zz} - \frac{1}{2}(\sigma_{xx} + \sigma_{yy})$] is vastly reduced due to the onset of plasticity. This response is shown for the case of $U_p = 0.9$ km s^{-1} in Fig. 2. We present below our analysis of the plasticity mechanisms involved in this shear stress release.

A. Fourier transform analysis

For some decades x-ray diffraction has been a tool of choice for the study of structure, and indeed microstructure, in crystalline samples. It is therefore of interest to look at the simulated response of the material in reciprocal space (the analogous computational technique) as a route to understanding microstructure within the simulations.[26] Indeed, this has proven to be a highly fruitful approach in previous studies.[3,5,10]

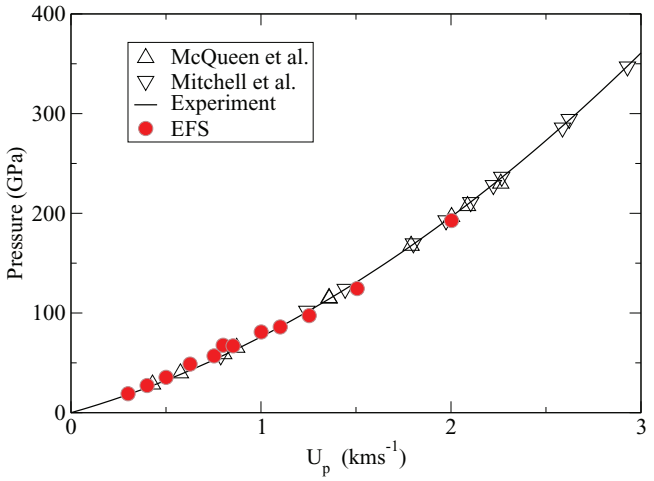

FIG. 1. (Color online) The experimentally determined Hugoniot compared with that for the EFS potential for shocks along [001]. Experimental data come from McQueen *et al.* (Ref. 24) and Mitchell *et al.* (Ref. 25), with the solid line being a fit to both data sets.

In a monatomic solid one can define the structure factor as

$$S(\mathbf{k}) = \sum_n e^{i\mathbf{k}\cdot\mathbf{r_n}}, \tag{1}$$

where $\mathbf{k}$ is a reciprocal space wave vector and $\mathbf{r_n}$ are the coordinates of the atoms in a certain region of interest. This is essentially a discrete Fourier transform (FT) of the atomic positions. Applying this technique gives rise to the

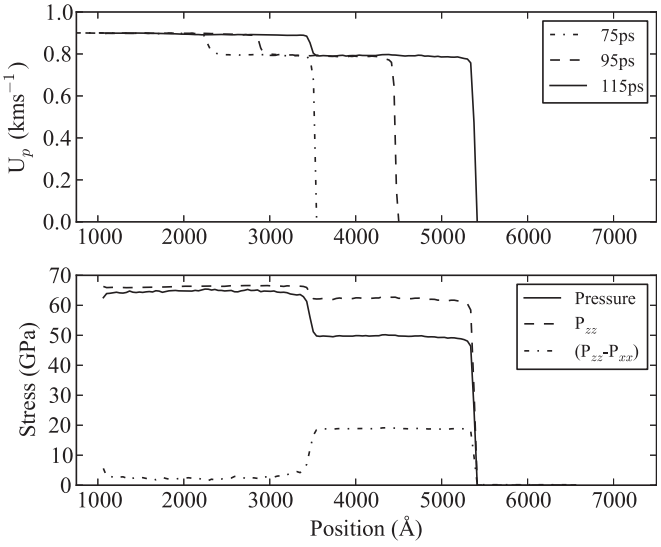

FIG. 2. Wave profiles for the $U_p = 0.9$ km s^{-1} simulation at an initial temperature of 5 K. The upper graph shows particle velocity profiles for several time steps, with labels indicating the time passed since the initial piston impact. The lower graph shows the pressure p_{zz} and shear stress for the 115 ps step. For this step the elastic front is seen around 5400 Å and the plastic (twinning) front at around 3500 Å. The profiles were calculated by averaging over atoms in 40 Å thick slabs (in the z direction).

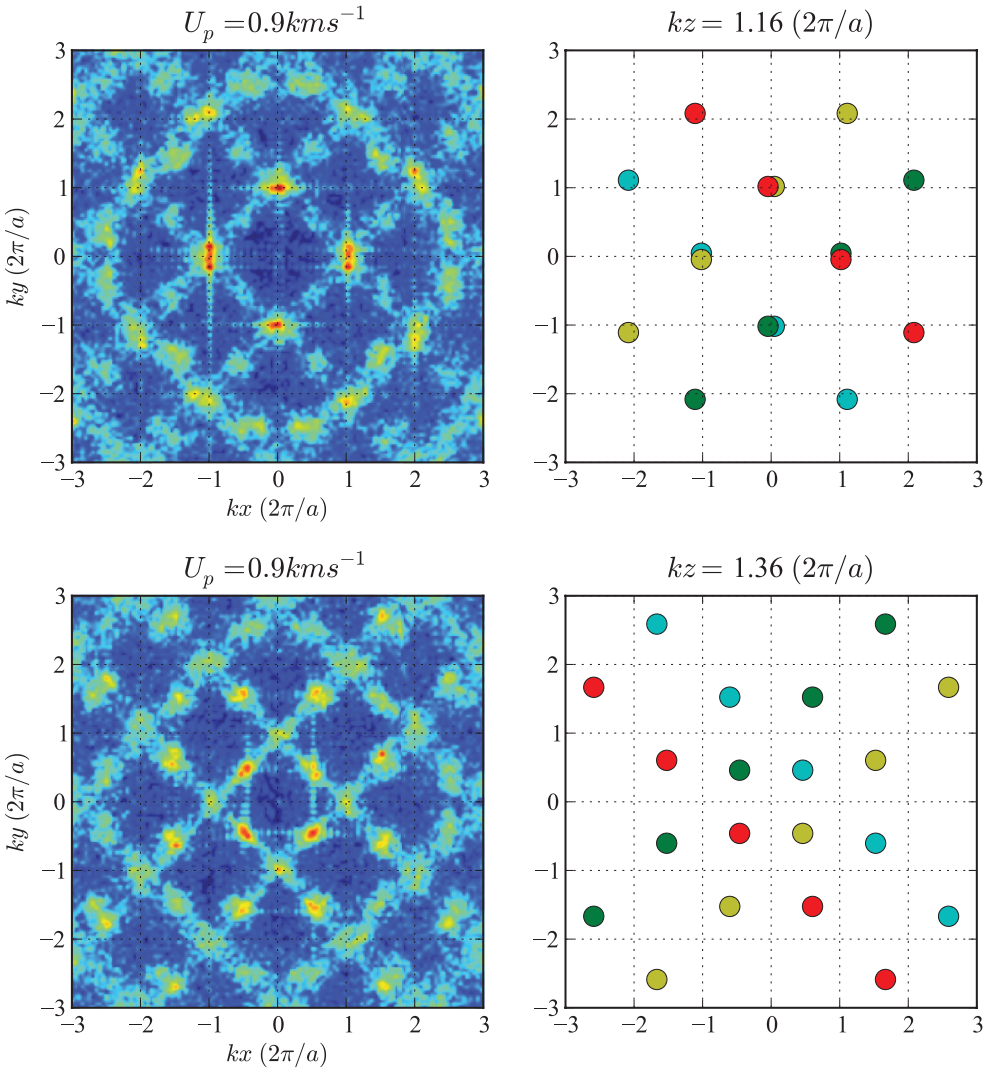

FIG. 3. (Color online) Intensity in the $k_z = 1.16\frac{2\pi}{a}$ and $k_z = 1.36\frac{2\pi}{a}$ planes showing the presence of a twinned region within the simulation. The lattice parameter for the unshocked material is used. The area shown ranges from $-3 \leqslant k(\frac{2\pi}{a}) \leqslant 3$ in both k_x and k_y, with color indicating intensity, blue being lowest and red being highest. The right hand plots show the various contributions to each peak from the four twin variants (red, yellow, green, and cyan). Note that many "diffraction spots" have contributions from more than one twin variant. Peaks seen in the intensity plot that are not identified in the right hand plot can be attributed to the finite width of other twin peaks lying slightly above or below the plane.

familiar reciprocal lattice, as well as features indicative of a microstructure. The intensity of the Fourier transform is calculated by taking the modulus squared $|S(\mathbf{k})|^2$, and is plotted in Fig. 3.

In Fig. 3 we show the FT, in the $k_z = 1.16\frac{2\pi}{a}$ and $k_z = 1.36\frac{2\pi}{a}$ planes, of a region of the sample compressed with a piston velocity of 0.8 km s^{-1} with $\frac{V}{V_0} \approx 0.8$. Note that due to the selection of a noninteger value of k_z, the uncompressed material does not contribute significantly to the signal in this plane. Figure 3 shows not only broad peaks consistent with the formation of small crystallites observed in real space (see Fig. 4), but the appearance of diffraction peaks inconsistent with pure uniaxial compression. This is indicative of a change in the structure, or orientation of parts of the sample. Note that at higher values of k there is a clear splitting of the peaks (masked at lower k due to the crystallite broadening). We associate the splitting of the peaks with the formation of twin variants in the four degenerate $\{112\}\langle 111\rangle$ twin systems expected in bcc material.[27] We identify which atoms are associated with each twin variant by use of a per atom structure factor, which then allows us to examine the strains and stresses associated with each variant, as well as within the untwinned material.

B. Per atom structure factor

The majority of extant analysis techniques for molecular dynamics rely on a degree of order in a system. Pair-correlation functions, although sometimes useful in determining structural changes such as a solid-solid phase transition, rapidly lose their sensitivity as the sample temperature or defect content increases.[28] Per atom order parameters such as coordination

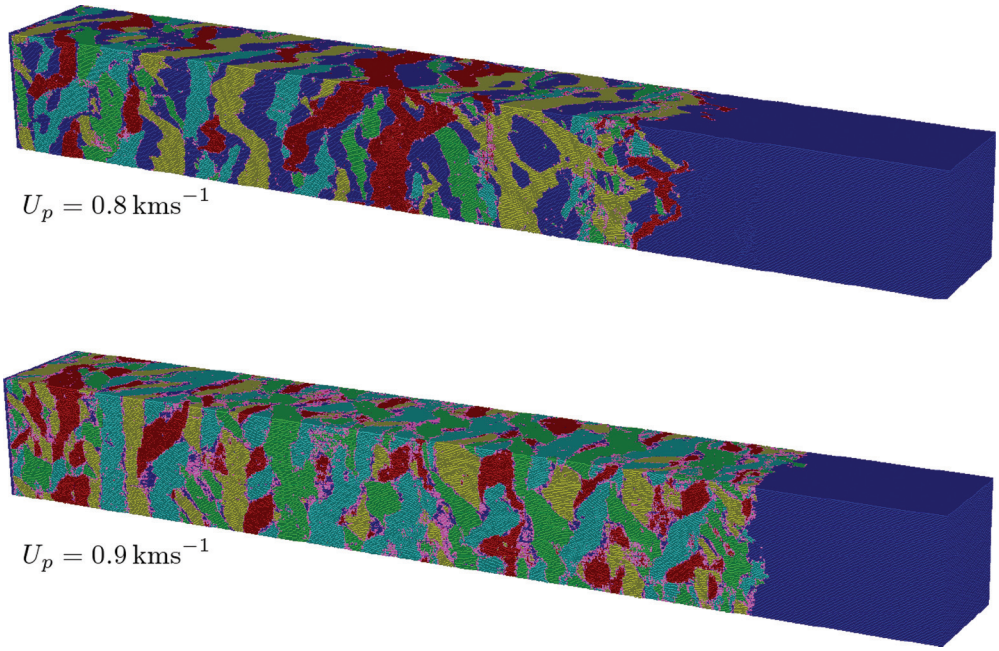

FIG. 4. (Color online) Two MD simulations with piston velocities of 0.8 and 0.9 km s^{-1}, initially thermalized at 5 K. The shown sample cross section is 425×425 Å^2. Color denotes the results of a categorization algorithm based on the PASF. Blue represents the untwinned orientation with green, red, cyan, and yellow denoting the twinned orientations. The atoms colored pink denote atoms where the orientation is not resolved, predominantly lying on the twin boundaries.

number, Ackland structure parameter,[29] atomic rotation,[30] and centrosymmetry parameter (CSP),[31] although intrinsically local, may not always discriminate between the various structures present in a highly disordered sample. For example, CSP in particular has been highly successful in identifying both line and planar defects in otherwise perfect fcc crystals,[3,12] but was found to fail for the twin boundaries present in these simulations. Since these per atom quantities are generally scalar in nature they do not convey any information on the orientation of, or the strains within, the sample. Fourier transforming of coordinates (effectively calculating the structure factor), although computationally expensive, does mitigate a number of these issues. It is relatively insensitive to temperature and disorder at the level we expect to find in shocked samples. It is also able to determine structure, rotations, and strains. However, it is nonlocal, and thus only has limited spatial resolution.

In order to address these potential shortcomings we introduce an intermediate technique, the per atom structure factor (PASF). This technique allows us to take advantage of a number of the powerful features of the Fourier transform while retaining the resolution and discrimination offered by a per atom parameter. We once again make use of the definition of the structure factor given in Eq. (1). For a conventional Fourier transform, such as those presented in Sec. II A, the sum would be over all atoms in some extended region. This is advantageous as the peak width in the structure factor is inversely proportional to the width of the sampling region. However, this increased k-space resolution comes at the cost of decreased real space precision. In order to produce a per atom quantity we take the sum over n to include the atom in question as well as all atoms within a spherical region around it. The size of this region is chosen so as to achieve an optimal balance of real and k-space resolutions for the problem at hand (for example, in this case we chose a region of 4 Å radius, equal to $\sim 1.2\,a_0$). Under larger compressions, the radius could be reduced to maintain real space resolution.

Although one could, in theory, use the information contained in the PASF to determine the full local structure of each atom (a concept similar to Voronoi analysis[32,33]), we choose here to select only a few representative k-space points for each atom. This more targeted approach relies on us having some understanding of the material response *a priori*. However, in the case of deformation twinning, the strict constraints on material orientation allow such a simplification.

By assuming that the twinned material is hydrostatically compressed, in the usual $\{112\}\langle 111\rangle$ system, and that the densities of twinned and host (that is to say, the material in the twinned region which had remained in its original orientation) materials are both close to the measured compressed bulk density, one can estimate the positions of Bragg peaks arising from both twinned and host materials. These estimates were found to be well representative of peak positions found in the full FT of the twinned region with some modest deviations being indicative of possible residual shear and density or orientation variations.

In Fig. 3 we show the contributions of each twin (color coded as red, cyan, yellow, and green) to each reciprocal lattice spot. We can now understand the complex structure of some spots as being due to multiple partially overlapped contributions. However, crucially, many spots are unique to a single twin variant, or to the host. This allows the identification of five peaks in reciprocal space (one for each twin, one for the host) which are indicative of a specific orientation of material. It should be noted that the PASF technique is improved by

using exact peak positions from the FT rather than our initial estimates.

We now perform the PASF technique for each of these points. Equation (1) is evaluated at each of the five k points for each atom in turn. For a given atom the sum is conducted over only those neighbors within 4 Å. These five PASF values are then compared. If one value is found to be significantly (in this case, at least a factor of 5) higher than any other value, the atom is said to belong to the corresponding orientation (a specific twin or the host). For a small number of atoms we find that two or more PASF points have comparable intensity. In this case we consider the atom to be part of a region with indeterminate orientation. This material is mainly confined to twin boundaries. In this way we can isolate the four twins, and the host, even in highly strained systems with just a modest set of initial assumptions about the material response.

III. ANALYSIS

Figure 4 shows two simulations colored according to the PASF as described in Sec. II B. The first figure shows a shock with $U_p = 0.8$ km s^{-1} corresponding to 57 GPa. Note that even just above the elastic limit we are seeing significant twinning fractions of around 70%. The twins nucleate at the second wave front, and quickly grow until meeting another twin. At longer time scales, the region behind the front is stable, after some initial equilibration between adjacent twins (see the movie in the Supplemental Material[34]). The boundaries between the twins are largely incommensurate, forming where two twinned regions grow into each other, and relatively few commensurate boundaries are observed in these larger simulations. Where commensurate boundaries do form, they are flat over many nm. In simulations with smaller cross sections (e.g., 120 × 120 Å^2), the growth of the twins through the periodic boundaries leads to a more regular structure of flat twinned regions with planar boundaries.[34] It should be noted that the PASF leads to a remarkably clean identification of twins, allowing the sample to be split into its constituent twin variants for further analysis. It was confirmed that these were indeed the four $\{112\}\langle 111\rangle$ variants by calculating the FT for each in turn.

By identifying which atoms are associated with a particular twin variant (or untwinned material) we can investigate the evolution of the large initial stresses and uniaxial strains, and how they are accommodated during twinning. From Fig. 2 we know that globally the shear stress is significantly relieved, but that on its own tells us little about what is happening locally within each crystallite. One might posit that the act of twinning allows each crystallite to relax back towards the hydrostat, in the sense that the local unit cell tends towards becoming cubic (rather than tetragonal as under uniaxial strain), thus reducing the shear strain of the sample both locally and globally. Such an accommodation could take place by allowing the twin boundaries to take up the plastic strain, but in doing so, one would expect to see the coherence of the boundaries compromised. An alternative mechanism could be dislocation generation and flow. However, the relatively high energy barrier for dislocation formation, and their low mobility, lead to a requirement for large dislocation densities which have typically been absent in simulations on this time scale.[35]

TABLE I. The von Mises stresses and normal strains of the host lattice and twin variants after twinning has relaxed the shear stress.

U_p (km s^{-1})	Material	von Mises stress (GPa)	ϵ_{xx}	ϵ_{zz}
0.8	Elastic	15.6	0.0	−0.165
	Untwinned	1.7	−0.046	−0.119
	Twin average	1.7	−0.057	−0.104
	Total	1.6		
0.9	Elastic	18.7	0.0	−0.173
	Untwinned	3.7	−0.050	−0.130
	Twin average	2.2	−0.056	−0.130
	Total	2.3		

One could also consider a situation (especially on the short time scales accessible to MD and even to picosecond x-ray diffraction experiments) where the initial uniaxial elastic strain (leading to a tetragonal unit cell in the elastically compressed material) is to a certain extent preserved, but in the act of twinning this tetragonal cell is rotated, leading to a situation where each twin still supports its own shear stress. The rotation of the strain and stress will effectively act to reduce the global shear stress.

The twinned region was sampled at the latest time step (140 ps), where the twins are fully stable. We find that the twinned material is supporting significant strain anisotropies $[\varepsilon_{zz} - \frac{1}{2}(\varepsilon_{xx} + \varepsilon_{yy})]$ of 4%–7% in the rotated coordinates of the cells, as shown in Table I. These values should be compared with the initial elastic compression of 16%–17%. The von Mises stress, $P_{\mathrm{VM}} = \{\frac{1}{2}[(P_{xx} - P_{yy})^2 + (P_{yy} - P_{zz})^2 + (P_{zz} - P_{xx})^2 + 6(P_{xy}^2 + P_{xz}^2 + P_{yz}^2)]\}^{1/2}$, of 15.6 GPa in the elastically compressed region, is reduced to 1.7 GPa in the twins. This local shear stress is close to the global shear stress, $P_{zz} - P_{xx}$. This suggests a model lying between the two situations described above, where the uniaxial strain is partly retained by the twins, but where shear stress is also locally relieved. The von Mises stress is higher than would be expected for the strains shown in Table I, thus suggesting some additional shearing of the tetragonal cell, during twinning or subsequent relaxation.

In the case of $U_p = 0.9$ km s^{-1} (65 GPa), the twinning fraction is over 95%. Once again, there is a large strain anisotropy, of approximately 7%–8%, in the twins and the remaining small fraction of untwinned material. The von Mises stress in the twins is once again close to the global value of 2.4 GPa, as one would expect due to the high twinning fraction. Again, there appears to be some degree of shearing of the cell as evidenced by the higher than expected von Mises stress given the observed strains.

The twinning fractions observed in these simulations are considerably higher than one might expect to observe in a real Ta sample, allowing us to study the twinning mechanism in isolation. In experiments, preexisting dislocation sources will contribute to relieve shear stress along with twins.[7] The simulations were repeated with the addition of voids to act as dislocation sources, and it was found that they were not enough to relieve the shear stress before the onset of twinning. In addition, it should be noted that we see no evidence for transformation to the ω phase in this pressure range, and

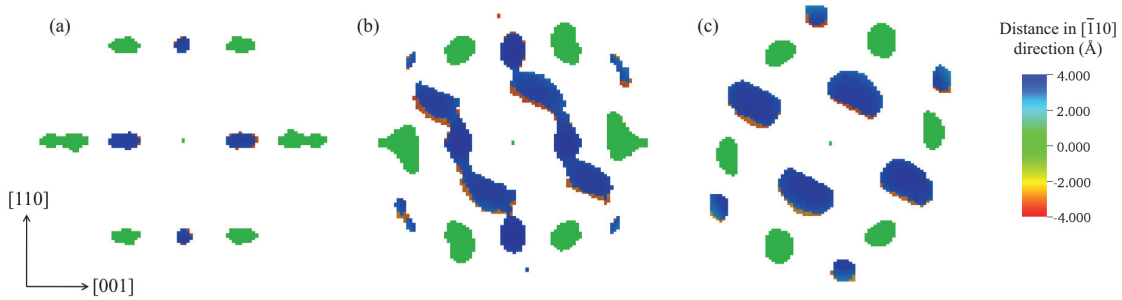

FIG. 5. (Color online) 3D pair-correlation function for atoms evolving from the host lattice to one of the four twin variants in the $U_p = 0.9$ km s^{-1} simulation. (a)–(c) show structure factors for the same atoms at simulation times of 10, 30, and 60 ps, respectively. Atoms chosen were those identified as being in the chosen twin at 140 ps as determined by the PASF. The coloring represents distance in the [$\bar{1}$10] direction, where green is in the plane, blue is one plane out of the page, and red is one plane below the page. The same pattern is observed for $U_p = 0.8$ km s^{-1}.

neither do we see unphysical face-centered-tetragonal (fct) material as previous studies using the Dai EFS Nb potential have reported.[36] In fact, Ravelo *et al.* showed that the EFS Ta potential has an artificial phase transition at 69 GPa, but our results focus on pressures below that transition.[21]

A. Mechanism

The mechanism employed in deformation twinning has long been a topic of some debate.[27] Although twinning is usually described in terms of shearing (or rotations) of the host lattice to a commensurate structure, it is not necessarily clear that these models adequately explain the mechanisms on the microscopic scale. In order to determine the mechanism for twinning we employ a three-dimensional (3D) pair-correlation function $g(\mathbf{r}) = \sum_i \sum_n \delta(\mathbf{r_n} - \mathbf{r_i} - \mathbf{r})$, where the sum in i covers all atoms in the sample, and n the neighbors of atom i falling within some radius of interest.[37] This technique has the advantage of preserving the directional information usually lost in forming the traditional scalar pair correlation $g(r)$. The function $g(\mathbf{r})$ is calculated by taking each atom in the sample in turn, considering it as a central atom, and calculating the displacements vectors of all neighboring atoms within the cutoff (in this case, 4 Å). These displacement vectors are binned into a 3D grid, effectively forming a representative, "average" unit cell for a region of the sample. Any motion of atoms is clearly seen as a trail of density originating at the initial position of the atoms, leading to the new position. In this way, the microscopic reordering of the average unit cell can clearly be identified.

The 3D pair-correlation function for one twinned variant (identified by the PASF) is shown in Fig. 5. The coloring in the figure indicates the distance along [$\bar{1}$10], i.e., the blue points are a plane out of the page. The three time steps correspond to the elastically compressed stage, during twinning, and the final twinned orientation. Figure 5(b) shows that relative to each ($\bar{1}$12) plane, the adjacent ($\bar{1}$12) planes are displaced, indicated by the streaking of the blue peaks, but the position of the next set of ($\bar{1}$12) planes (green) is largely unchanged. In the standard shearing mechanism for twinning, these outer ($\bar{1}$12) planes are displaced, suggesting that another mechanism is occurring.

When the elastic compression before twinning is taken into account, the reason that alternating ($\bar{1}$12) planes remain largely stationary becomes clear. The measured compression for the simulation with piston velocity $U_p = 0.9$ km s^{-1}, in the elastically compressed region $3500 < z < 5400$ Å, is 18%. At this compression the atoms on alternating (112) planes are almost coincident with the equivalent positions in the twin (at $\epsilon_{zz} = \sqrt{2/3} - 1$ these positions are exactly coincident, ignoring thermal vibrations). Therefore, at this compression, only every other (112) plane must shift. This is illustrated in Fig. 6. Under this mechanism, the initial uniaxial strain is rotated into the twin orientation. This would lead to the rapid relief of global shear stress seen in the wave profile in Fig. 2. The twinned material then relaxes elastically towards the strains shown in Table I, reducing the shear stress further, as seen in the shear stress profile.

The direction in which each alternate (112) plane shifts is not obvious and two potential mechanisms are shown in Fig. 6 by the red and blue arrows. In order to confirm the direction of shuffling on the alternate planes, the relative displacements

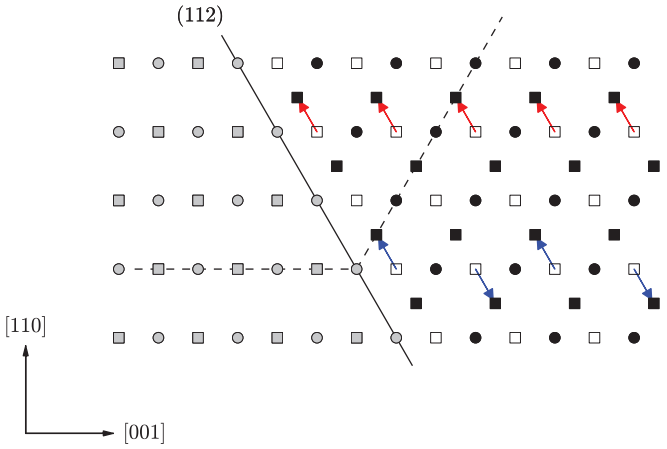

FIG. 6. (Color online) The proposed shuffle mechanism for shock compression with this potential, with an initial compression of 18.4%. Squares and circles represent two neighboring (1$\bar{1}$0) planes. Gray sites denote the host lattice, with white and black sites indicating the initial and final positions of the twinned atoms. Twin boundaries are indicated by solid lines with a dashed line highlighting the twin. The red and blue arrows indicate two potential shuffle mechanisms that cause the ($\bar{1}$12) planes to shift in the same or alternating ⟨111⟩ directions.

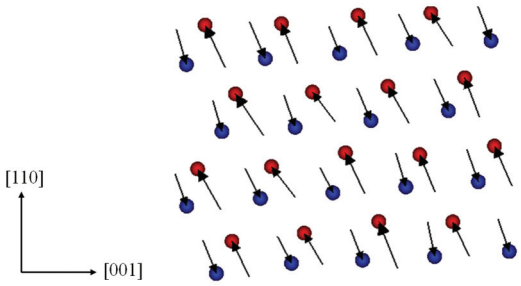

FIG. 7. (Color online) Relative displacements for a small region of one twin variant. The arrows indicate the change in position, between 80 and 120 ps, for each atom with respect to its nearest neighbor in the $[0\bar{1}0]$ direction. Red and blue spheres represent atoms in two neighboring $(1\bar{1}0)$ planes.

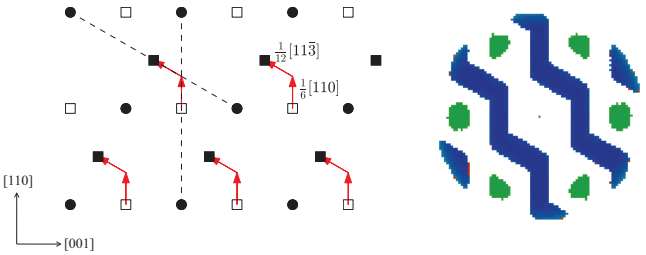

FIG. 8. (Color online) Twinning mechanism showing the path taken by the atoms, implying two partial dislocations with Burgers vectors $\frac{1}{6}[110]$ and $\frac{1}{12}[11\bar{3}]$. The right part of the figure shows the 3D pair-correlation function for this idealized mechanism, which can be compared to Fig. 5(b).

of the atoms were visualized, and this is shown in Fig. 7. For each atom, its position with respect to its neighbor in the $[0\bar{1}0]$ direction is compared for two different time steps, producing a relative displacement. This method was chosen as there is no obvious frame of reference to use in the shock simulation to subtract the large change of position in the shock direction. The displacement vectors are plotted with heads lying at the atom positions in the latter time step. The time steps were chosen such that the region is elastically compressed in the first time step, and twinned in the second time step. The result shows that each (112) plane is displaced in the opposite direction to the two neighboring (112) planes. This is compatible with the mechanism indicated by the red arrows in Fig. 6, where alternating (112) planes are displaced in the same direction.

The 3D pair-correlation function shown in Fig. 5(b) shows that the atoms do not take a straight path to the twin positions. The two (112) planes adjacent to the origin are streaked with a particular curvature. This curvature is approximated by the path shown in Fig. 8. The atoms move along the [110] and then along the $[11\bar{3}]$ direction. It should be noted that although this path goes through a position equivalent to an hcp phase, no bulk hcp material was seen in the FT. The density of the 3D pair-correlation function at the hcp equivalent position is low, seen in Fig. 5(b) as the nodelike points of the streaked regions, suggesting the hcp material is not present. These directions are transverse to the compression direction in the original and rotated coordinates, respectively, indicated by the dashed lines in the figure. Additionally, Fig. 8 shows the 3D pair-correlation function produced where the atoms have been artificially displaced according to this mechanism, which is qualitatively similar to Fig. 5(b).

This mechanism could be directly driven by phonon softening or instability. However, there is no significant softening of the relevant modes in the EFS potential up to compressions of 0.7. This suggests that the barrier to twinning has not been artificially reduced due to pathologies in the high pressure behavior of the potential, as has been observed elsewhere.[38]

IV. CONCLUSIONS

Molecular dynamics simulations of shock compression of Ta with piston velocities of $U_p = 0.8$ and 0.9 km s^{-1} and employing the EFS potential show significant deformation twinning. By employing a per atom structure factor method to identify the four variants we can study the detailed stress and strain responses of both untwinned and twinned materials. Large strain anisotropies, and associated shear stresses, are identified locally in the material. In addition, we unambiguously determine the twinning mechanism, finding short range shuffling of alternate (112) planes to be responsible for bulk reordering of the material. Although potentially driven by phonon mode softening, we see no evidence for this in the EFS potential up to the highest pressure studied here. The method for twin detection is applied to the specific case of bcc material, modeled with a particular potential, and shocked along the [001] direction. The method would work for identifying twinning for shocks in other directions, and is a general procedure which could also be applied to study other structures and modes of deformation, for example, (polymorphic) phase transitions, where the new phase orientation is related to the original phase orientation.

ACKNOWLEDGMENTS

A.H. and M.S. are grateful for support from AWE. E.M.B. is thankful for support from PICT2008-1325. The authors thank Yizhe Tang for useful discussions.

*m.suggit1@physics.ox.ac.uk

[1]T. C. Germann, B. L. Holian, P. S. Lomdahl, and R. Ravelo, Phys. Rev. Lett. **84**, 5351 (2000).

[2]E. M. Bringa, J. U. Cazamias, P. Erhart, J. Stolken, N. Tanushev, B. D. Wirth, R. E. Rudd, and M. J. Caturla, J. Appl. Phys. **96**, 3793 (2004).

[3]E. M. Bringa, K. Rosolankova, R. E. Rudd, B. A. Remington, J. S. Wark, M. Duchaineau, D. H. Kalantar, J. Hawreliak, and J. Belak, Nat. Mater. **5**, 805 (2006).

[4]G. Kimminau, B. Nagler, A. Higginbotham, W. J. Murphy, N. Park, J. Hawreliak, K. Kadau, T. C. Germann, E. M. Bringa, D. H. Kalantar, H. E. Lorenzana, B. A. Remington,

and J. S. Wark, J. Phys.: Condens. Matter **20**, 505203 (2008).
[5]W. J. Murphy, A. Higginbotham, G. Kimminau, B. Barbrel, E. M. Bringa, J. Hawreliak, R. Kodama, M. Koenig, W. McBarron, M. A. Meyers, B. Nagler, N. Ozaki, N. Park, B. Remington, S. Rothman, S. M. Vinko, T. Whitcher, and J. S. Wark, J. Phys.: Condens. Matter **22**, 065404 (2010).
[6]R. Chau, J. Stolken, P. Asoka-Kumar, M. Kumar, and N. C. Holmes, J. Appl. Phys. **107**, 023506 (2010).
[7]C.-H. Lu, B. R. Maddox, B. A. Remington, E. M. Bringa, M. Kawasaki, T. G. Langdon, H.-S. Park, B. Kad, and M. A. Meyers, in *Proceedings of the Conference of the American Physical Society Topical Group on Shock Compression of Condensed Matter*, edited by M. L. Elert, W. T. Buttler, J. P. Borg, J. L. Jordan, and T. J. Vogler, AIP Conf. Proc. No. 1426 (AIP, Melville, NY, 2011), p. 1387.
[8]M. J. Suggit, A. Higginbotham, J. A. Hawreliak, G. Mogni, G. Kimminau, P. Dunne, A. J. Comley, N. Park, B. A. Remington, and J. S. Wark, Nat. Commun. **3**, 1224 (2012).
[9]K. Kadau, T. C. Germann, P. S. Lomdahl, and B. L. Holian, Science **296**, 1682 (2002).
[10]J. Hawreliak, J. D. Colvin, J. H. Eggert, D. H. Kalantar, H. E. Lorenzana, J. S. Stölken, H. M. Davies, T. C. Germann, B. L. Holian, K. Kadau, P. S. Lomdahl, A. Higginbotham, K. Rosolankova, J. Sheppard, and J. S. Wark, Phys. Rev. B **74**, 184107 (2006).
[11]D. H. Kalantar, J. F. Belak, G. W. Collins, J. D. Colvin, H. M. Davies, J. H. Eggert, T. C. Germann, J. Hawreliak, B. L. Holian, K. Kadau, P. S. Lomdahl, H. E. Lorenzana, M. A. Meyers, K. Rosolankova, M. S. Schneider, J. Sheppard, J. S. Stölken, and J. S. Wark, Phys. Rev. Lett. **95**, 075502 (2005).
[12]K. Kadau, T. C. Germann, P. S. Lomdahl, R. C. Albers, J. S. Wark, A. Higginbotham, and B. L. Holian, Phys. Rev. Lett. **98**, 135701 (2007).
[13]J. A. Hawreliak, B. El-Dasher, H. Lorenzana, G. Kimminau, A. Higginbotham, B. Nagler, S. M. Vinko, W. J. Murphy, T. Whitcher, J. S. Wark, S. Rothman, and N. Park, Phys. Rev. B **83**, 144114 (2011).
[14]N. Gunkelmann, E. M. Bringa, K. Kang, G. J. Ackland, C. J. Ruestes, and H. M. Urbassek, Phys. Rev. B **86**, 144111 (2012).
[15]J. A. Shields, S. H. Goods, R. Gibala, and T. Mitchell, Mater. Sci. Eng. **20**, 71 (1975).
[16]R. W. Anderson and S. E. Bronisz, Acta Metall. **7**, 645 (1959).
[17]L. E. Murr, M. A. Meyers, C.-S. Niou, Y. J. Chen, S. Pappu, and C. Kennedy, Acta Mater. **45**, 157 (1997).
[18]L. M. Hsiung and D. H. Lassila, Acta Mater. **48**, 4851 (2000).
[19]J. M. McNaney, L. M. Hsuing, N. R. Barton, and M. Kumar, in *Proceedings of the American Physical Society Topical Group on Shock Compression of Condensed Matter*, edited by M. L. Elert, M. D. Furnish, W. W. Anderson, W. G. Proud, and W. T. Buttler, AIP Conf. Proc. No. 1195 (AIP, Melville, NY, 2009), p. 1127.
[20]S. Plimpton, J. Comput. Phys. **117**, 1 (1995).
[21]R. Ravelo, Q. An, T. C. Germann, and B. L. Holian, in *Proceedings of the Conference of the American Physical Society Topical Group on Shock Compression of Condensed Matter*, edited by M. L. Elert, W. T. Buttler, J. P. Borg, J. L. Jordan, and T. J. Vogler, AIP Conf. Proc. No. 1426 (AIP, Melville, NY, 2011), p. 1263.
[22]X. D. Dai, Y. Kong, J. H. Li, and B. X. Liu, J. Phys.: Condens. Matter **18**, 4527 (2006).
[23]J. A. Moriarty, J. F. Belak, R. E. Rudd, P. Söderlind, F. H. Streitz, and L. H. Yang, J. Phys.: Condens. Matter **14**, 2825 (2002).
[24]R. G. McQueen and S. P. Marsh, Los Alamos Science Laboratory Report No. GMX-6-566, 1964.
[25]A. C. Mitchell and W. J. Nellis, J. Appl. Phys. **52**, 3363 (1981).
[26]G. Kimminau, B. Nagler, A. Higginbotham, W. Murphy, J. Wark, N. Park, J. Hawreliak, D. Kalantar, H. Lorenzana, and B. Remington, in *Proceedings of the Conference of the American Physical Society Topical Group on Shock Compression of Condensed Matter*, edited by M. Elert, M. D. Furnish, R. Chau, N. Holmes, and J. Nguyen, AIP Conf. Proc. No. 955 (AIP, Melville, NY, 2007), p. 1251.
[27]J. W. Christian and S. Mahajan, Prog. Mater. Sci. **39**, 1 (1995).
[28]G. Kimminau, Ph.D. thesis, University of Oxford, 2009.
[29]G. J. Ackland and A. P. Jones, Phys. Rev. B **73**, 054104 (2006).
[30]R. E. Rudd, Mater. Sci. Forum **633–634**, 3 (2009).
[31]C. L. Kelchner, S. J. Plimpton, and J. C. Hamilton, Phys. Rev. B **58**, 11085 (1998).
[32]I.-F. W. Kuo and C. J. Mundy, Science **303**, 658 (2004).
[33]W. Brostow, M. Chybicki, R. Laskowski, and J. Rybicki, Phys. Rev. B **57**, 13448 (1998).
[34]See Supplemental Material at http://link.aps.org/supplemental/10.1103/PhysRevB.88.104105 for a movie of deformation twinning, in a bcc single crystal, shocked in the [001] direction ($U_p = 0.9$ km s^{-1}).
[35]Y. Tang, E. M. Bringa, B. A. Remington, and M. A. Meyers, Acta Mater. **59**, 1354 (2011).
[36]R. F. Zhang, J. Wang, I. J. Beyerlein, and T. C. Germann, Philos. Mag. Lett. **91**, 731 (2011).
[37]X. Cheng, J. H. McCoy, J. N. Israelachvili, and I. Cohen, Science **333**, 1276 (2011).
[38]G. Kimminau, P. Erhart, E. M. Bringa, B. Remington, and J. S. Wark, Phys. Rev. B **81**, 092102 (2010).